FLOW-INDUCED BIREFRINGENCE MEASUREMENT SYSTEM USING DUAL-CRYSTAL TRANSVERSE ELECTRO-OPTIC MODULATOR FOR MICROGRAVITY FLUID PHYSICS APPLICATIONS

Jeffrey R. Mackey, NYMA, Inc. NASA Lewis Group
2001 Aerospace Parkway, Brook Park, Ohio 44142 , jmackey@lerc.nasa.gov

ABSTRACT

We have developed a new instrument that can measure fast transient birefringence and polymer chain orientation angle in complex fluids. The instrument uses a dual-crystal transverse electro-optic modulator with the second crystal's modulation voltage applied 180° out of phase from that of the first crystal. In this manner, the second crystal compensates for the intrinsic static birefringence of the first crystal, and it doubles the modulation depth. By incorporating a transverse electro-optic modulator with two lithium-niobate (LiNbO3) crystals oriented orthogonal to each other with a custom-designed optical system, we have produced a very small, robust instrument capable of fast transient retardation measurements. By measuring the sample thickness or optical path length through the sample, we can calculate the transient birefringence. This system can also measure dichroism.

We have compared the calibration results and retardation and orientation angle measurements of this instrument with those of a photoelastic modulator (PEM) based system using a quarter wave plate and a high-precision 1/16-wave plate to simulate a birefringent sample. Transient birefringence measurements on the order of 10^{-9} can be measured using either modulator.

INTRODUCTION

Existing polarimeters traditionally incorporate either a single-crystal PEM or a rotating retardation plate as the modulator element. Although these systems are capable of very sensitive birefringence and dichroism measurements, they are either too large or too fragile to survive the forces encountered by space-based experiments during launch and landing on board the STS or sounding rockets. For example, sounding rocket launch loads are typically on the order of 17g. In order to obtain the desired sensitivity while maintaining a stable and rugged configuration, we suggest using a dual-crystal transverse electro-optic modulator (EOM) geometry. The modulator crystals must be oriented with their principal axes orthogonal to each other and at ±45° with respect to the polarization state of the incident light. The drive voltage applied to the second crystal must be 180° from that of the first crystal. The suggested optical configuration is shown in figure 1.
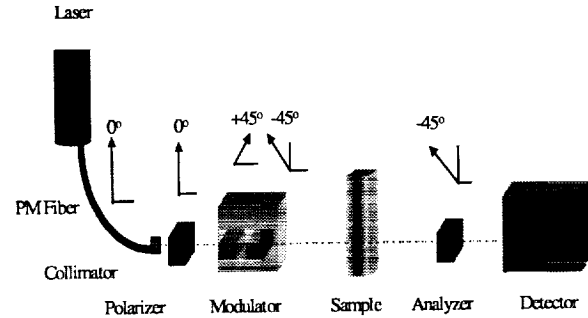
Figure 1. Birefringence Measurement System showing polarization and dual-crystal modulator geometry.

Transverse electro-optic modulators can be made very small, rugged and lightweight. LiNbO3 crystals are non-hygroscopic, and they can be mounted in a resonant circuit to reduce electrical power needed to drive the modulator. These are all highly desirable qualities when designing an experiment suitable for space flight.

We have demonstrated through the Mueller matrix calculations and by experimentation how to design a flight-worthy electro-optically modulated birefringence measurement system. We show that the retardation and thus the birefringence of an optically transparent fluid polymer can be measured accurately using this novel technique.

OVERVIEW OF BIREFRINGENCE

Birefringence (Δn') is the difference in a material's refractive index with respect to the polarization state of light propagating through it. In an optically transparent stressed polymer material, the orientation and degree of deformation of the molecular polymer chains cause an anisotropic polarization. If the light propagates through a birefringent material along the z-direction, the x and y components of its electric field vector will be different from one another. This results in a phase difference or retardation (δ) as the light traverses the sample material. If the material is not dichroic, then the retardation is related directly to its birefringence. This can be expressed as

$$\Delta n' = n_o - n_e = -\frac{\delta\lambda}{2\pi d} \qquad (1)$$

where n_o and n_e are the refractive indices for ordinary and extraordinary light rays respectively, λ is the vacuum wavelength of the light, and d is the sample material thickness.

One can apply this knowledge using the stress optic law, which provides a simple relationship between the material stress and the refractive index tensor. In terms of shear stress (τ_{xy}), the stress optic law can be expressed as

$$\tau_{xy} = \frac{1}{2}C\Delta n' \sin(2\chi(t)) \qquad (2)$$

where C is the materials stress optic coefficient and $\chi(t)$ is the time-variant orientation angle of the molecular polymer chains with respect to the flow or stress direction. Thus, in order to measure a material's shear stress, we must measure the birefringence and average molecular chain orientation angle simultaneously.

THEORY OF DUAL CRYSTAL TRANSVERSE ELECTRO-OPTIC MODULATION

We developed a dual-crystal modulation technique using the Stokes parameters and Mueller matrix representations of the optical elements. We implemented the theory using the transverse electro-optic effect or Pockel's effect and its application to the LiNbO$_3$ crystals as two separate Mueller matrices.

A birefringent crystal possesses two distinct indices of refraction. These indices are represented by n_o and n_e, which are the ordinary and extraordinary index of refraction, respectively. When a voltage is applied across the crystal in a direction normal to the direction of light propagation, the difference between polarization-sensitive refractive indices changes. This change results in a voltage-sensitive phase retardation between the ordinary and extraordinary light rays, which can be mathematically expressed as

$$\Delta\phi = \frac{2\pi}{\lambda}(n_o - n_e)L - \frac{2\pi}{\lambda}r_{33}n_o^{\,3}\frac{VL}{D} \qquad (3)$$

where r_{33} is the appropriate electro-optic coefficient, L is the crystal length, D is the distance between electrodes and V is the voltage applied across the crystal. If V is an alternating voltage, we can modulate the electric field vector or polarization state of the light passing through the crystal. For pure LiNbO$_3$, n_o=

2.2866 and n_e= 2.2028 at 20°C*. A transverse electro-optic crystal configuration is shown in figure 2.
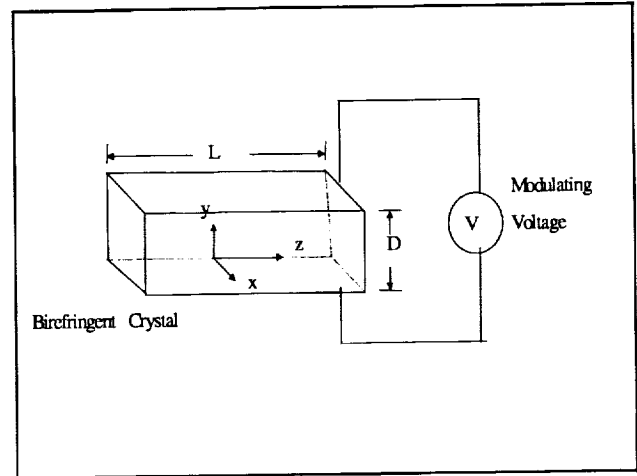
Figure 2. Transverse electro-optic modulator geometry. Light propagates in the z-direction. We apply modulation voltage in the ±y-direction.

From equation (3), we can see that the electro-optic effect is maximized when the electric field vector of plane-polarized light is incident on the left crystal face at a 45° angle with respect to the z-axis. We can also observe that there is static birefringence that depends largely on crystal length L. In many crystals, including LiNbO$_3$, this static birefringence is highly temperature dependent[2,4]. We have experimented with single-crystal LiNbO$_3$ modulators and have measured the effective static retardation to be 2.24×10^{-2} radians in a 40mm length crystal at 20°C. We see that this retardation corresponds to a static birefringence of 5.69×10^{-8} radians. Although the crystal's static birefringence is quite small, it is not thermally stable[2]. One may use a single-crystal transverse electro-optic modulator in this type of instrument, but the instrument must be operated in a temperature-stabilized environment. The temperature-dependent static birefringence is an undesirable property since it reduces the instrument's sensitivity and stability when measuring very small birefringence levels in a sample material. Fortunately, by using the dual-crystal configuration shown in the preceding figure 1, we can compensate for both the residual static birefringence and the thermal instability while doubling the modulation depth.

In order to derive how this geometry works, we need to describe how polarized light interacts with the optical elements. Since light is an electromagnetic wave,

---

* From Manufacturer's data sheet.

511

the Stokes vector, S that consists of four parameters, can characterize its polarization state. These parameters are I, Q, U, and V, which are based on the electric field vector.

$$S = \begin{bmatrix} I \\ Q \\ U \\ V \end{bmatrix} = \begin{bmatrix} (Ex(t))^2 + (Ey(t))^2 \\ (Ex(t))^2 - (Ey(t))^2 \\ 2Ex(t)Ey(t)\cos(\delta) \\ 2Ex(t)Ey(t)\sin(\delta) \end{bmatrix} \quad (4)$$

In equation (4), Ex(t) and Ey(t) are the time-dependent x and y electric field vector components, and δ is the instantaneous phase retardation between $-\pi$ and $+\pi$. The parameter I, represents the intensity of the light while the parameters Q, U, and V specify its state of polarization.

The polarization state of an optical system can be modeled using the Stokes vector of the incident light multiplied by the Mueller matrices of the individual optical elements. The multiplications are done in reverse order to generate the output Stokes vector that yields information about the subject material under study. That is, if we represent the incident light with the Stokes vector [S_i] and have polarization optical elements represented by their 4x4 Mueller matrices [Analyzer], [Sample] and [Modulator] as shown in figure 3, the output Stokes vector is computed as

$$[S_{out}] = [Analyzer][Sample][Modulator][S_i]. \quad (5)$$

For the dual-crystal polarimeter in our experiment, we have the following polarization state configuration shown in figure 3. All angles are referenced looking into the laser. We define the input polarization at zero degrees. The dual-crystal transverse electro-optic modulator crystals are at $\pm45°$ and the analyzer is at $-45°$ with respect to the input polarization state.
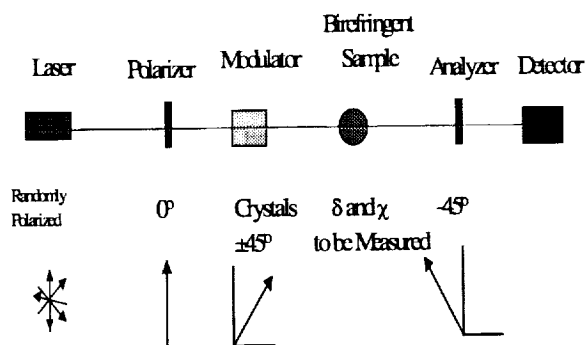
We multiplied the representative Mueller matrices in reverse order to calculate an equivalent system matrix that was then multiplied by the input Stokes vector. The resulting Stokes vector describes the intensity and polarization of the light emerging from the last element in the system matrix. Once equation (5) is computed using the matrix elements, it is Fourier-Bessel expanded so that I(t) can be written in terms of quantities measurable by two heterodyning lock-in amplifiers The time-variant intensity, I(t), is given by the first element of the resultant Stokes vector and is given below.

$$I(t) = Idc[1 + 2J_1(A_0)\sin(\omega t)\sin(\delta(t))\cos(2\chi(t))$$
$$+ 2J_2(A_0)\cos(2\omega t)\{1 - \cos(\delta(t))\}\sin(2\chi(t))\cos(2\chi(t))$$
$$+ ...]$$
$$(6)$$

where $A_0 = 2.4048$. Equation (6) gives us I(t) in terms of the in-phase and in-quadrature signal components.

INSTRUMENT STABILITY

Since thermal stability is a major problem for a single-crystal LiNbO$_3$ transverse electro-optic modulator, we performed stability tests. We configured the system with the input polarizer at 0°, the single-crystal modulator at +45°, and the analyzer at –45°. We placed a quarter wave plate in the sample space and rotated it to give approximately 1/16 wave retardation. This is where the I_ω and $I_{2\omega}$ signals are equal. We then separated these signals slightly by rotating the quarter wave plate a few degrees. We increased the laboratory temperature by 10°F over a period of 16 hours. We recorded data over this period to observe the signal variance. The stability of the single-crystal modulator is very poor due to the temperature dependence of the intrinsic birefringence of lithium niobate[4]. We then repeated this test using a dual-crystal LiNbO$_3$ modulator. Figure 4 shows the results of both tests.

Figure 3. Polarization state representation of optical elements.

Stability Test for Single Crystal EOM
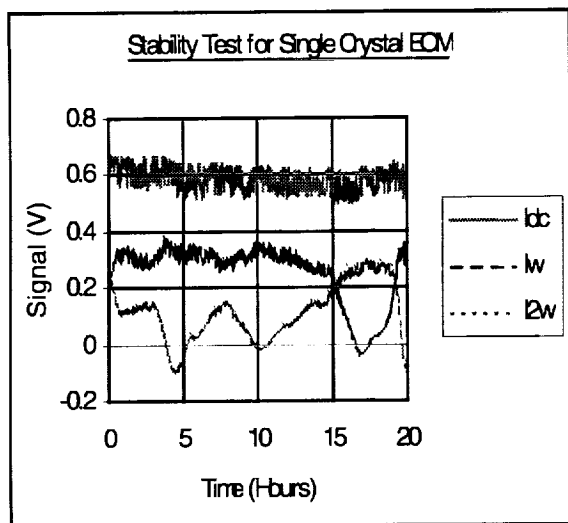
Figure 4a. *Long term stability test results for a single-crystal EOM. The plots show the photodetector and lock-in amplifier signal outputs. Idc is the dc signal plus the detector bias voltage while $I\omega$ and $I2\omega$ are the first and second harmonic signals respectively.*

Stability Test using Dual-Crystal EOM
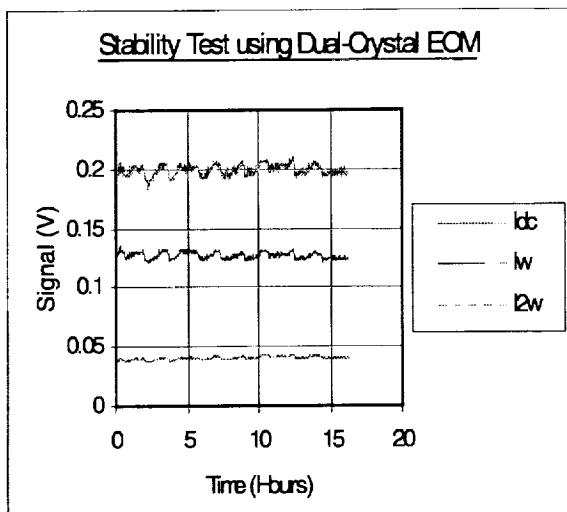
Figure 4b. *Long term stability test results for a dual-crystal EOM. The plots show the photodetector and lock-in amplifier signal outputs. Idc is the dc signal plus the detector bias voltage while $I\omega$ and $I2\omega$ are the first and second harmonic signals respectively.*

INSTRUMENT CALIBRATION

Since we wanted to set the instrument where $J_0(A)=0$, we performed a standard "zero-Bessel calibration" as described in reference 6. This method involves the

measurement of the dc signal while incrementing the modulation voltage for three different retardation values in the sample space. The results are shown in figure 5a.
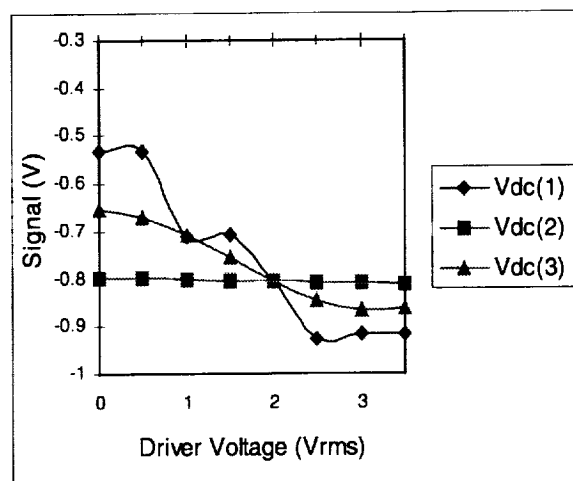
Figure 5a. *"Zero-Bessel" plot to calibrate for $J_0(A)=0$. In this case, the dc signal is plotted against modulation voltage for three different retardation values in the sample space.*

We observe that the approximate modulation voltage setting is 2V. This calibration method is subject to noise in the dc signal and is not as accurate as we would want.

There are several other ways to calibrate this system, but perhaps the most useful method is one that maps out the Bessel functions $J_1(A)$ and $J_2(A)$ simultaneously, yielding a full calibration sweep instead of just a single-point calibration measurement. With the instrument configured so that the input polarizer is at $0°$, the electro-optic modulator crystals are at $\pm45°$, and the analyzer is at $-45°$, we place a retardation plate in the sample space. As long as the retarder is oriented such that the first and second harmonic signals are present, we may increment the modulation voltage, record the in-phase and in-quadrature lock-in amplifier output signals, and scale these accordingly to observe their correlation with $J_1(A)$ and $J_2(A)$. The parameter A is proportional to the modulation voltage. The calibration plot then gives us our modulation voltage at any desired Bessel function value. We plotted the correlation between our electro-optic modulator and the theoretical Bessel function values in figure 5b.

513
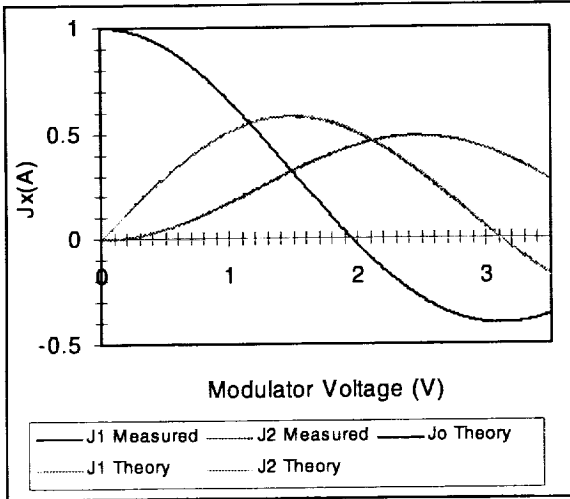
Figure 5b. Calibration curves generated using a dual-crystal transverse electro-optic modulator. Modulation voltage was incremented from 0 to 3.5V rms with the modulation frequency held constant at 42KHz.

From the figure 5b calibration plot, we may more accurately observe that $J_0(A)=0$ when our modulation voltage is approximately 1.95V rms. The calibration plots determine the correct modulation voltage where $J_0(A)=0$.

By setting the modulation voltage such that $J_0(A)=0$, we can easily obtain the sample retardation, $\delta(t)$ and sample orientation angle, $\chi(t)$. In this case, the value of A is 2.4048. The Bessel function calibration values are given as $J_0(A)=0$, $J_1(A)=0.5191$ and $J_2(A)=0.4317$.

MEASUREMENT RESULTS

We took measurements of the retardation and orientation angle of a rotating quarter wave plate using the electro-optically modulated system and the same optical system incorporating a photoelastic modulator (PEM) in place of the EOM. The intrinsic static strain retardation of the dual-crystal EOM was 3.85×10^{-4} while that of the PEM was an order of magnitude greater. We placed a quarter wave retardation plate in the sample space. We altered the retardation and orientation angle using a piezo-driven rotary mount to rotate the retardation plate at constant angular velocity. The dc signal component as well as the first two harmonics were recorded to calculate retardation and orientation angle simultaneously. These measurement results are shown in figure 6. We generated these plots using the Extensional Rheology Experiment flight prototype optical assembly. The optical assembly consists of a diode laser head, laser-to-fiber coupler, polarization-maintaining optical fiber, collimating

microlens, beam splitter polarizer cube, polarizer/collimator mounting assembly with rotational adjustment capability, beam splitter analyzer cube, analyzer housing with rotational adjustment capability, analyzer-to-detector mounting fixture, and a high-speed silicone pin-diode based photodetector. All of these components were used in the optical configuration to compare performance between the PEM and EOM systems. The only component that we changed for this comparison was the modulator itself.
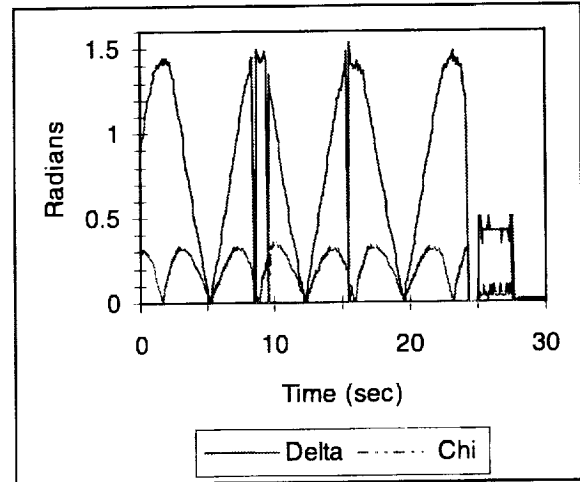
Figure 6a. Retardation (Delta) and Orientation Angle (Chi) vs. Time for a rotating quarter wave plate in the PEM-based system.
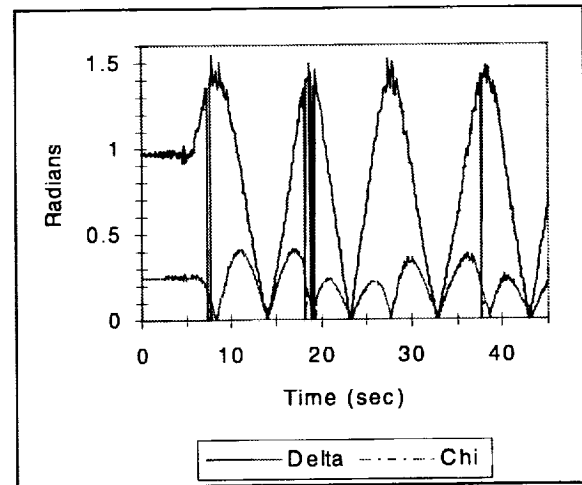
Figure 6b. Retardation (Delta) and Orientation Angle (Chi) vs. Time for a rotating quarter wave plate in the EOM-based system.

The figure 6 plots give the retardation ranging from zero to $\pi/2$ and the orientation angle ranging from zero

to $\pi/8$. The slight variation in the orientation angle on the figure 6b plot is due to the inability to rotate the EOM to the correct angle on our breadboard system. A very slight deviation leads to many other terms in the output Stokes vector. The orientation angle calculation is very sensitive to these terms. The final flight system design will correct this problem by enabling rotational alignment of the EOM.

To get a more accurate measurement of the retardation, we placed a precision $\pi/8$ (0.3927 radians) plate in the sample space. This retardation plate has a tolerance of ±0.001 waves or ±0.0063 radians according to the manufacturer. The PEM-based system measured the retardation at 0.401 radians while the EOM-based system measured it at 0.396 radians.

DISCUSSION AND CONCLUSIONS

We have developed a stable transverse electro-optically modulated birefringence measurement system suitable for microgravity fluid physics applications. The experimental results from the dual-crystal EOM compare favorably with those of the PEM. They also agree within the accepted tolerances of the retardation plates used. This type of modulation scheme has many advantages over existing modulation schemes. Advantages include variable modulation frequency from 0 to 100MHz, low power consumption, low mass, small size, and an extremely rugged package. The only potential disadvantage is that $LiNbO_3$ may experience photorefractive damage with high-powered lasers.

Due to its small size, this type of system may be useful in many types of terrestrial and microgravity applications where experiment space is very limited.

ACKNOWLEDGEMENTS

REFERENCES

1. Frattini, Paul L, Galante, Stephen R. and Chilcote, Steven M, "Practical Aspects of Polarization Modulated Flow Birefringence: A Technique-Oriented Review", Carnegie Mellon University, (1990).
2. "Practical Uses and Applications of Electro-Optic Modulators", New Focus, Inc, *Application Note # 2*.
3. Walker, M. J., "Matrix Calculus and the Stokes Parameters of Polarized Radiation", *J. Optical. Soc. Am.*, pp. 170-174, (1954).
4. Denton, R. T., Chen, F. S. and Ballman, A. A., "Lithium Tantalate Light Modulators", *Journal of Applied Physics*, Vol. 38, Number 4, pp. 1611-1617, March, (1967).
5. McKinley, G. H. and Spiegelberg, S. H., "The Extensional Rheology of Non-Newtonian Materials", Third Annual Microgravity Fluid Physics Conference, *NASA Conference Publication 3338*, pp. 377-382, (1996.)
6. Oakberg, T., "PEM-90™ Photoelastic Modulator Systems User Manual", Hinds™ Instruments, Inc., (1994).